PHYSICAL REVIEW D VOLUME 19, NUMBER 1 1 JANUARY 1979

Prism-plot analysis of the reaction $\pi^- p \to \pi^- \pi^- \pi^+ p$ at 13 GeV/c

J. A. Gaidos and W. L. Yen
Purdue University, West Lafayette, Indiana 47907 and Indiana University–Purdue University at Indianapolis, Indianapolis, Indiana 46205
(Received 30 June 1978)

Fourteen reaction channels contributing to the final state have been separated by a prism-plot analysis of $\pi^- p \to \pi^- \pi^- \pi^+ p$ interactions at 13.2 GeV/c. The results of this study are presented in terms of partial and differential cross sections, invariant-mass and decay-angular distributions, and comparisons with other separation techniques for the various resonant states.

I. INTRODUCTION

We present a study of the reaction

$$\pi^- p \to \pi^- \pi^- \pi^+ p \tag{1}$$

at 13.2 GeV/c wherein the technique of a prism-plot analysis[1] (PPA) is utilized to separate the contributions of noninterfering resonant channels and diffractive enhancements. This analysis is based on 16 804 events obtained from a 500 000 picture exposure of the SLAC 82-inch hydrogen bubble chamber. The data were measured on scanning measuring projectors and processed by standard TVGP and SQUAW reconstruction and fitting routines. Our cross section was measured to be 1.00 ± 0.04 mb.

Reaction (1) has been studied over a wide range of incident pion momenta in a series of bubble-chamber experiments.[2-15] Strong production of $\Delta^{++}(1236)$, A_1, A_2, and ρ substates is clearly observed at all energies. In addition, moderate contributions from f, A_3, $\Delta^0(1236)$, $N^*(1520)$, and $N^*(1688)$ are frequently resolved. These resonances and enhancements can be attributed to one of three dominant classes of reactions mechanisms: (i) pion diffractive dissociation, (ii) double resonance production, and (iii) proton diffractive dissociation. In particular, we enquire to what extent reaction (1) can be described in terms of resonant and diffractive channels.

One goal of phenomenological analyses of exclusive high-energy production reactions is to separate and study independently each different final state contributing to a specific set of constrained interactions. However, the techniques involving kinematical restrictions to isolate the dominant modes are not effective in selecting subsamples of events in the less pronounced channels. At our energy, a satisfactory separation of the three dominant reaction classes listed above is possible by longitudinal-phase-space analysis (LPSA).[16] However, in order to isolate different final states within the main classes, a technique with improved resolution, such as that provided by the PPA, is required. In the PPA, a complete set of independent phase-space variables is used to describe each event, which for reaction (1) involves seven variables. Simultaneous weighting in the independent variables provides a more powerful alternative to cuts in invariant mass and momentum transfer for selecting data samples corresponding to specific reaction channels. The PPA has been employed by several groups.[1, 15, 17-22]

We describe the performance of our analysis and present the results in terms of partial and differential cross sections and invariant-mass and decay-angular distributions for each of the 14 reactions comprising the data sample.

II. THE PPA METHOD

The PPA is an approach which employs the complete set of phase-space variables. An iterative comparison is performed between the unseparated experimental data sample and the Monte Carlo-generated samples which are based on the information obtained in the preceding step. The underlying scheme is that reaction channels produced via different types of interactions occupy different regions in the seven-dimensional phase space. The seven independent phase-space variables used herein are all evaluated in the overall center of mass and include the three Van Hove longitudinal-momentum variables,[16] the three independent variables from the Dalitz-Fabri kinetic energy simplex, and the transverse momentum of the final-state ($\pi^-\pi^-$) system. After transforming these variables to Cartesian coordinates, the prism-plot variables are utilized in the following combinations:

$$X_1 = \tfrac{1}{4}[3q_1 - (q_2 + q_3 + q_4)],$$

$$X_2 = \frac{1}{2\sqrt{2}}[2q_2 - (q_3 + q_4)],$$

$$X_3 = \frac{\sqrt{6}}{4}(q_3 - q_4),$$

$$X_4 = \tfrac{1}{4}[3T_1 - (T_2 + T_3 + T_4)],$$

$$X_5 = \frac{1}{2\sqrt{2}}[2T_2 - (T_3 + T_4)],$$

$$X_6 = \frac{\sqrt{6}}{4}(T_3 - T_4),$$

$$X_7 = |\vec{P}_{\perp 3} + \vec{P}_{\perp 4}|,$$

where q_n is the longitudinal momentum and T_n the kinetic energy of the nth particle with the indices $n = 1$ to 4 referring to final-state particles p, π^+, π^-, π^-, respectively. Taking into account the presence of two identical pions in the final state requires only sign changes of X_3 and X_6 to specify coordinates for the other combination.

The PPA proceeds via the following steps:

(1) From one- or two-dimensional projections of the experimental sample, guess the number K of different reaction channels to be included.

(2) For each reaction channel, choose a set of one-dimensional distributions such as invariant mass, production angles, or decay angles. The shapes of these distributions are obtained from the previous iteration, except the forms for resonant masses, for which Breit-Wigner distributions are adopted. For the initial iteration, flat angular distributions are assumed as well as a rectangular form for the diffractive proton mass enhancement, and a triangular shape for the mass distribution of pion diffractive dissociation.

(3) Beginning with equal numbers of events for each assumed reaction channel, generate K samples of Monte-Carlo events based upon the distributions of step (2) input; subsequent numbers of events per channel will be given by a weight W_i described below.

(4) Draw a seven-dimensional "box" of suitable size around each real event and count the number of Monte-Carlo events (hits) of each type which have phase-space location within that box (this process will be referred to as "tagging" the events).

(5) Assign to each real event a weight W_i^j defined as

$$W_i^j = \frac{\text{(number of hits from Monte Carlo events of type } i \text{ for the } j\text{th event)}}{\text{(total number of hits for the } j\text{th event)}},$$

$i = 1, K$; $j = 1, N$; where N is the number of real events. The weight W_i^j is the probability for the jth event belonging to the ith reaction channel. For the next iteration, the number of Monte-Carlo events generated for each reaction channel will be proportional to W_i where $W_i = \sum_j W_i^j$.

(6) By weighting the jth event of the data sample with the probability W_i^j, obtain the set of new distributions corresponding to those chosen in step (2). Examine the spectra of untagged events to ascertain whether there are structures indicative of omitted reaction channels. If additional final states are necessary, include them in the next iteration.

(7) Submit these new distributions to the Monte Carlo generation program.

(8) Repeat the sequence of steps (3) to (7) until convergence is achieved where the criterion is that the distributions following a certain iteration are statistically identical to those of the previous iteration. It is important during a single tagging process to utilize a set of different box sizes B_i in increasing order:

$$B_1 < B_2 < \text{---------} < B_k .$$

If N_1 of N events are tagged with respect to B_1, the remaining $(N - N_1)$ events will be attempted using B_2, etc. For the analysis described herein, six box sizes were used. Initially the box sizes were chosen small to obtain rapid convergence and to determine the approximate domain of population. Subsequently, the sizes were increased to insure complete coverage of the event sample.

The assumption of uncorrelated amplitudes in PPA is apparent from the preceding description. Interferences among particle amplitudes can be resolved subsequently by other techniques, for which the tagged data sample provides a very clean input.

III. CONTRIBUTING CHANNELS

The question of which reaction channels contribute to the experimental data and therefore have to be introduced into the Monte Carlo generation must be answered by the iteration process itself. Initially, the choice of channels is a conjecture derived from the original unseparated data sample and from a previous analysis of conspicuous states selected by kinematical cuts. Effective mass spectra of the unseparated data are shown in Fig. 1, where there is clear evidence

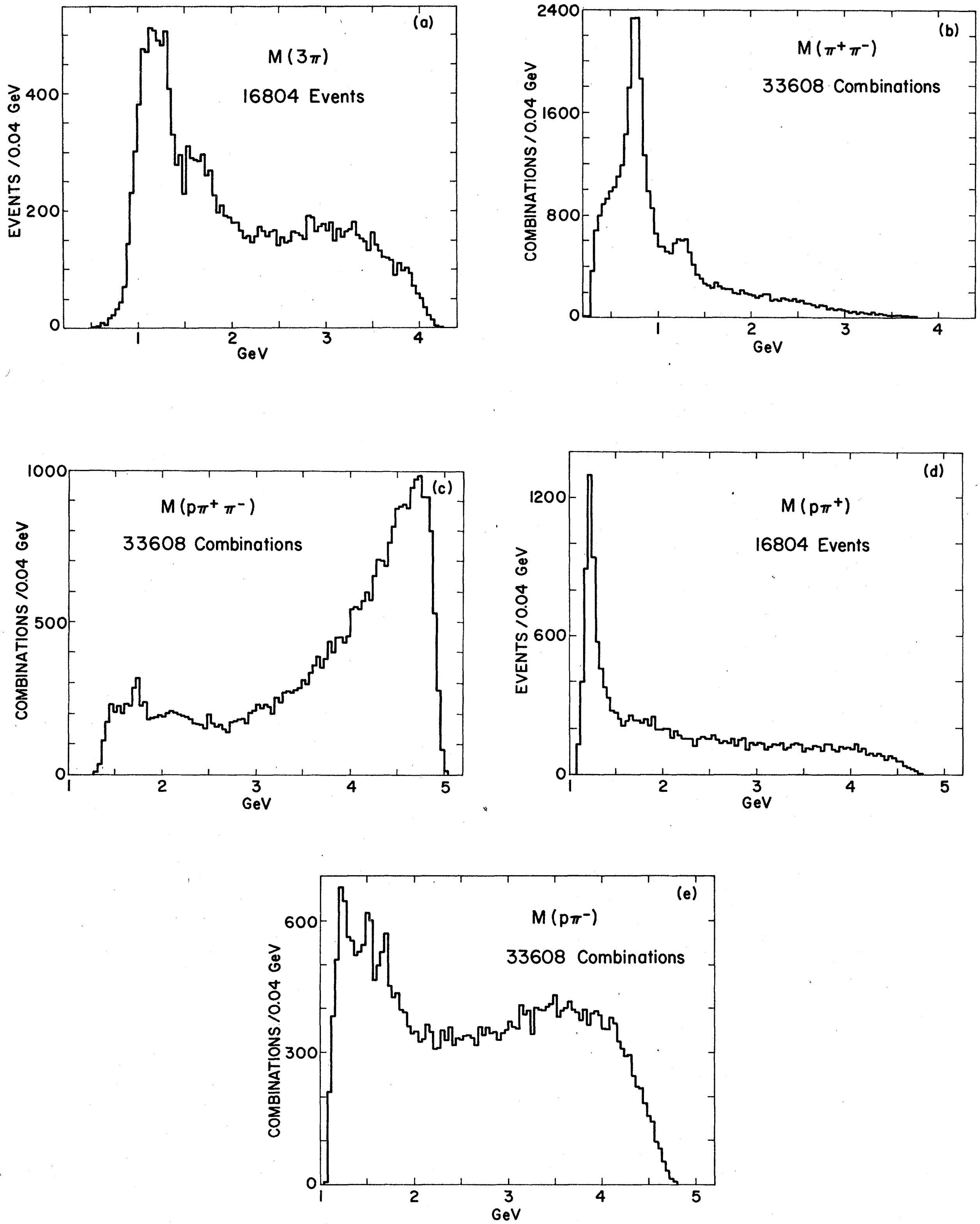

FIG. 1. Effective-mass distributions in the reaction $\pi^- p \rightarrow \pi^- \pi^- \pi^+ p$ at 13.2 GeV/c: (a) mass spectrum of the $\pi^- \pi^- \pi^+$ system; (b) mass spectrum of $\pi^+ \pi^-$ combinations, (c) mass spectrum of $\pi^- \pi^+ p$ combinations, (d) mass spectrum of $\pi^+ p$ system, (e) mass spectrum of $\pi^- p$ combinations.

TABLE I. Reaction channels considered and the corresponding partial cross sections obtained from the prism-plot analysis of $\pi^- p \to \pi^- \pi^- \pi^+ p$ at 13.2 GeV/c. The subscript DD indicates diffraction dissociation.

Reaction final state	Number of events	Cross section (μb)
1. pA_1^-, $A_1^- \to \rho^0 \pi^-$	3210	200 ± 17
2. pA_2^-, $A_2^- \to \rho^0 \pi^-$	2000	124 ± 13
3. pA_3^-, $A_3^- \to f \pi^-$	1135	71 ± 9
4. pA' (2000), $A' \to \rho^0 \pi^-$	1032	64 ± 9
5. $\Delta^{++} \pi^- \pi^-$	1077	67 ± 9
6. $\Delta^0 \pi^+ \pi^-$	281	17 ± 5
7. $\Delta^0 \rho^0$	624	39 ± 7
8. $\Delta^0 f$	526	33 ± 6
9. $\Delta^0 g$	461	29 ± 6
10. $N^*(1520)\rho^0$	863	54 ± 8
11. $N^*(1688)\rho^0$	1045	65 ± 9
12. $N^*(1688) f$	764	47 ± 7
13. $(p\pi^+\pi^-)_{DD}\pi^-$	1307	81 ± 10
14. $(\Delta^{++}\pi^-)_{DD}\pi^-$	1765	110 ± 12

for strong production of the Δ^{++} (1236) isobar, ρ^0 and A_2 mesons and the diffractive A_1 enhancement. There are also definite signals for f^0, A_3, Δ^0 (1236), $N^*(1520)$, and $N^*(1688)$ contributions. A listing of the included channels is given in Table I; masses and widths of resonances and the initial mass shapes of nonresonant contributions are specified in Table II.

TABLE II. Initial parameters for the reaction products. BW = Breit-Wigner distribution centered at M_0. △ = triangular distribution centered at M_0. □ = rectangular distribution centered at M_0. DD = diffraction dissociation.

Product	Mass shape	M_0 (MeV)	Width (MeV)
ρ	BW	770	150
f	BW	1270	180
g	BW	1690	180
A_1	△	1100	300
A_2	BW	1310	100
A_3	△	1600	200
A'	△	2000	200
$\Delta(1236)$	BW	1232	110
$N^*(1520)$	BW	1520	125
$N^*(1688)$	BW	1670	155
$(p\pi\pi)_{DD}$	□	1700	500
$(\Delta^{++}\pi^-)_{DD}$	□	1700	500

IV. RESULTS FROM THE PPA

Convergence in this analysis was attained after thirteen iterations, when the cross sections and differential distributions were observed to be statistically equivalent to those of the previous step. The number of events tagged by each channel included and the corresponding partial cross sections are listed in Table I. A residual of 714 events representing 4% of the data sample was not attributed to any of the considered channels and was consequently untagged. An examination of the mass spectrum (Fig. 2) reveals no significant structure indicative of channels overlooked. For cross sections quoted, these events are distributed proportionately among the fourteen tagged channels.

Invariant mass, four-momentum transfer, and decay angular distributions in the Gottfried-Jackson frame are shown for channels 1 → 14 in Figs. 3–15.

Previous studies of $\pi^-\pi^-\pi^+ p$ final states, especially partial wave analyses[6,13,23-26] have revealed interferences between adjacent production channels, in particular between A_1 and A_2 states. However, in the PPA analysis the A_1 and A_2 channels have been treated as noninterfering states. Consequently, the values presented in Table I for separate A_1 and A_2 channels are only an approximation and spectra for the sum of these channels are given in Fig. 3.

An interpretation of the results of this analysis is closely connected with the degree of separation achieved among the contributing reaction channels. A measure of the resolution obtained can be expressed in terms of a simple overlap matrix between channels i and j, M_{ij} (Ref. 20) defined by

$$M_{ij} = \frac{1}{N_i} \sum_{k=1}^{N} \left(1 - \frac{|W_i^k - W_j^k|}{W_i^k + W_j^k}\right).$$

Here N_i is the total number of events with nonzero W_i^k. Elements M_{ij} are proportional to the amount of common phase space for channels i and j; however, because $N_i \neq N_j$, the overlap matrix is not symmetric. Values of the various M_{ij} are listed as percentages in Table III. With few exceptions, the overlap elements are well below ten percent, thus indicating that the separation of mechanisms contributing to reaction (1) is satisfactory. Major overlaps in phase space occur for the proton diffractive subsample, the A_1 and A_2 channels, and the $N^*(1520)\rho^0$ and $N^*(1688)\rho^0$ final states.

Slope parameters, assuming an exponential t' dependence, are given in Table IV. for each of the reaction channels, for two t' intervals.

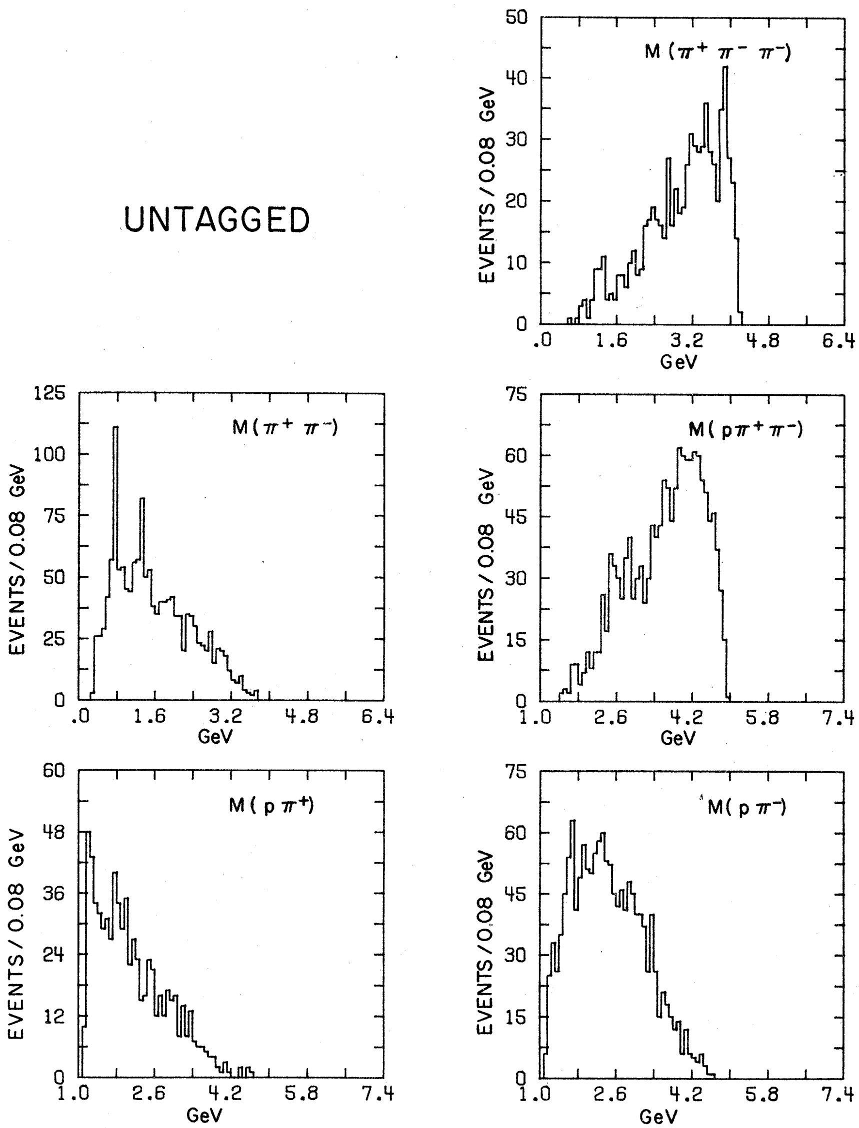

FIG. 2. Effective-mass distributions of residual (untagged) events not associated with a specific reaction channel.

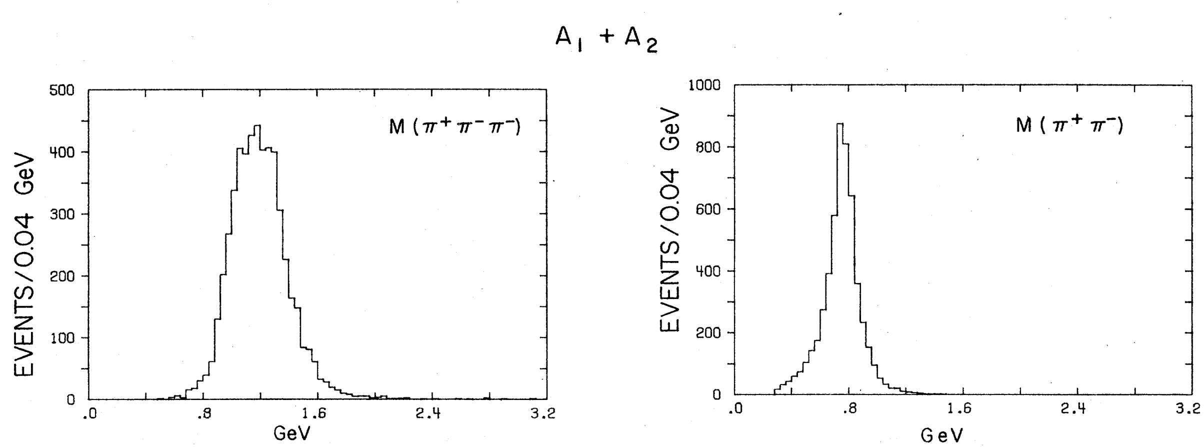

FIG. 3. Effective-mass distributions for the reactions $\pi^- p \to (A_1 \text{ or } A_2)\, p$ with subsequent $A_{1,2}^- \to \rho\pi^-$ decay.

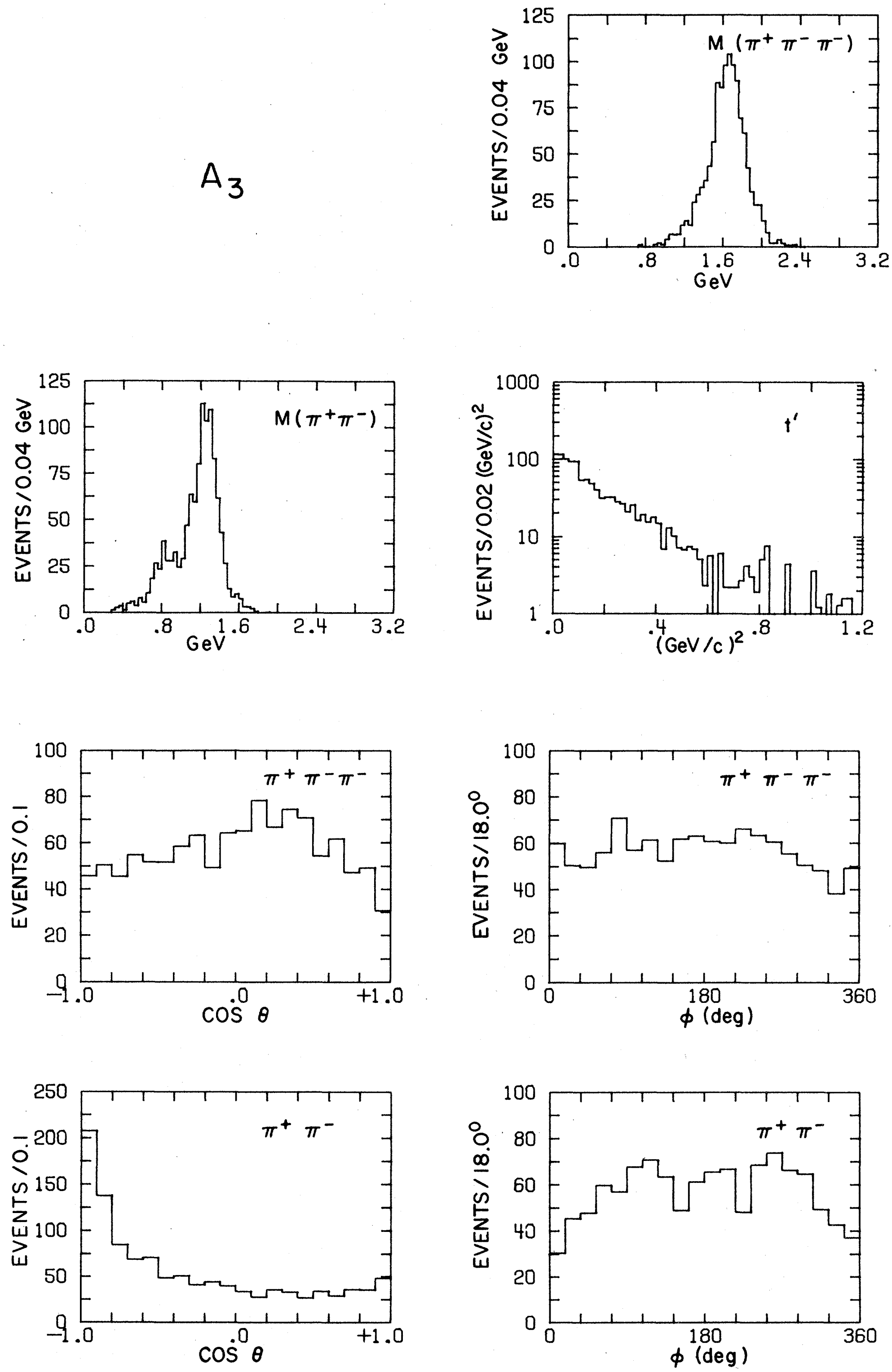

FIG. 4. Effective-mass, momentum-transfer, and decay-angular distributions for the reaction $\pi^- p \to A_3^- p$ with $A_3^- \to f\pi^-$ decay.

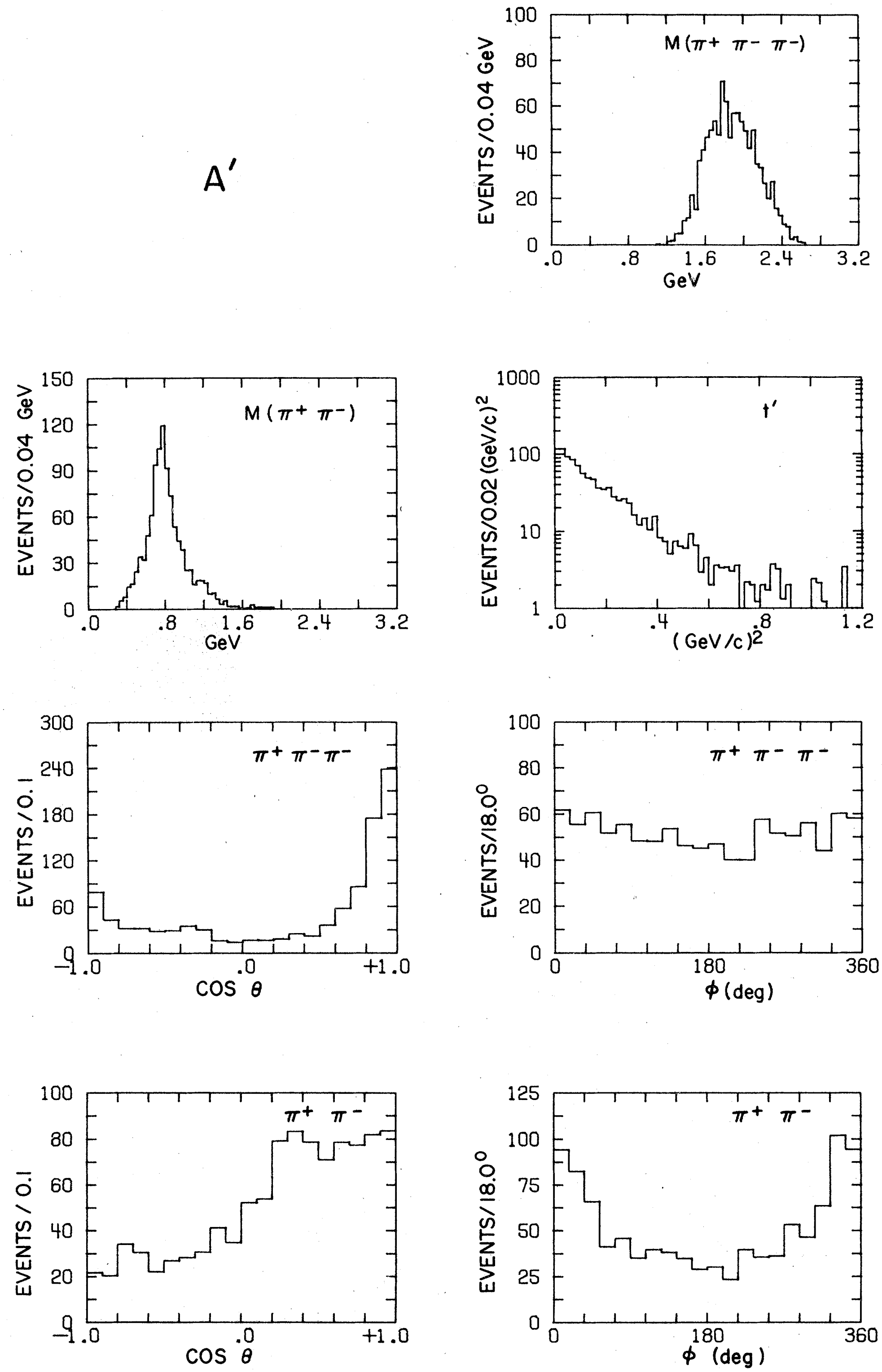

FIG. 5. Effective-mass, momentum-transfer, and decay-angular distributions for the reaction $\pi^- p \to A'(2000)\, p$ with $A'(2000) \to \rho\pi^-$ decay.

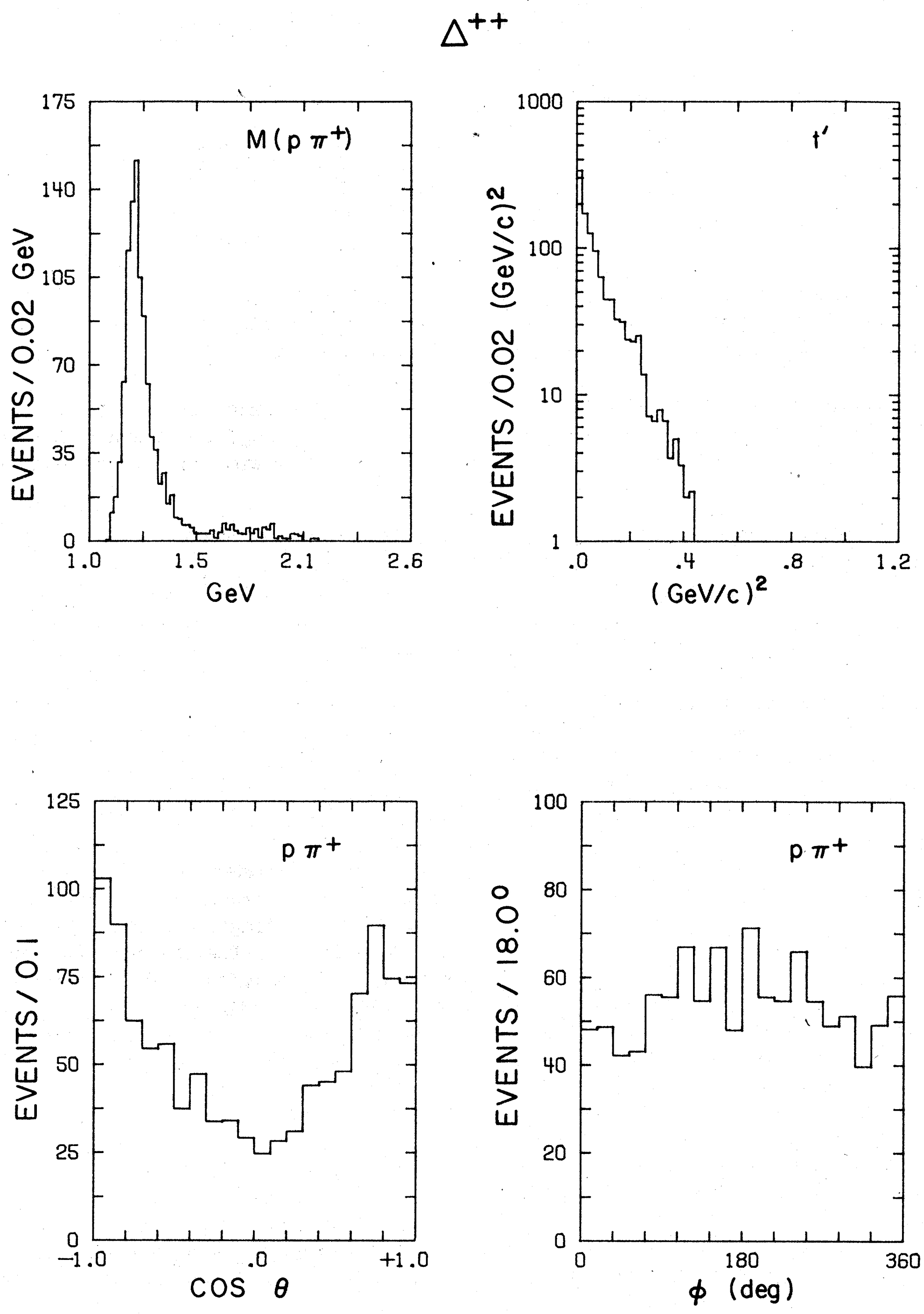

FIG. 6. Effective-mass, momentum-transfer, and decay-angular distributions of the Δ^{++} in the reaction $\pi^- p \to \Delta^{++} \pi^- \pi^-$.

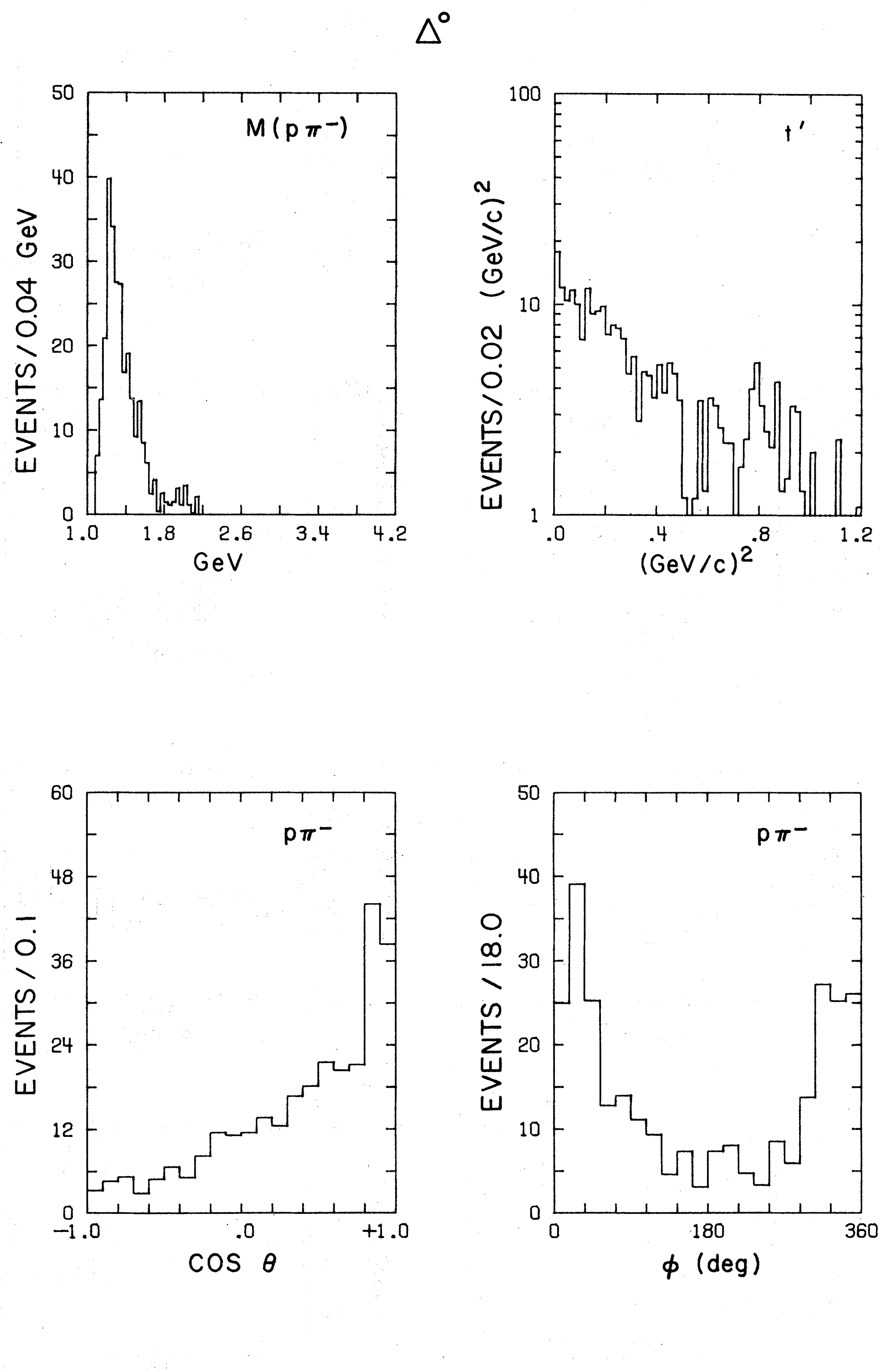

FIG. 7. Effective-mass, momentum-transfer, and decay-angular distributions of the Δ^0 in the reaction $\pi^- p \to \Delta^0 \pi^+ \pi^-$ for nonresonant $\pi^+\pi^-$ combinations.

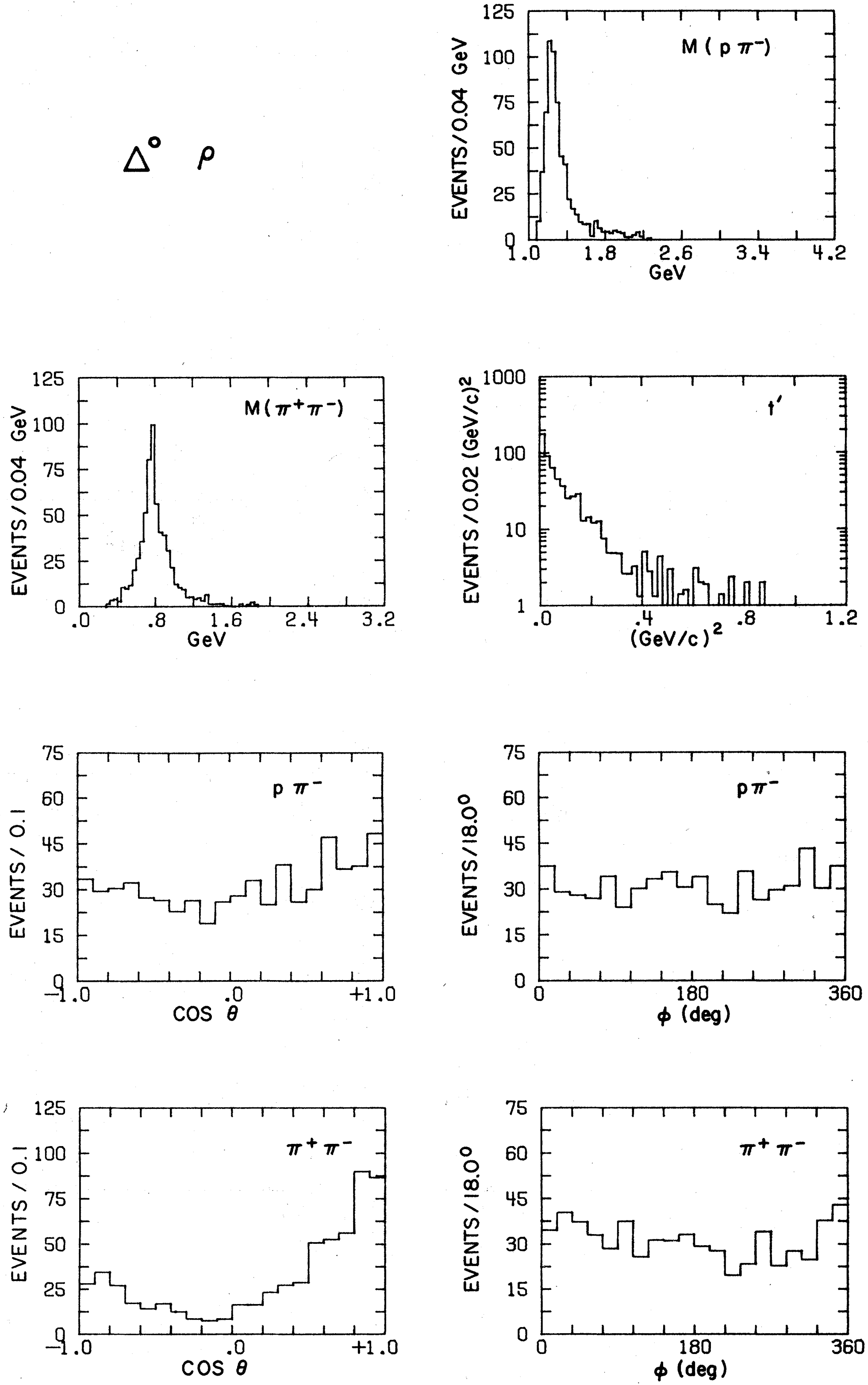

FIG. 8. Effective-mass, momentum-transfer, and decay-angular distributions for the reaction $\pi^- p \to \Delta^0 \rho^0$.

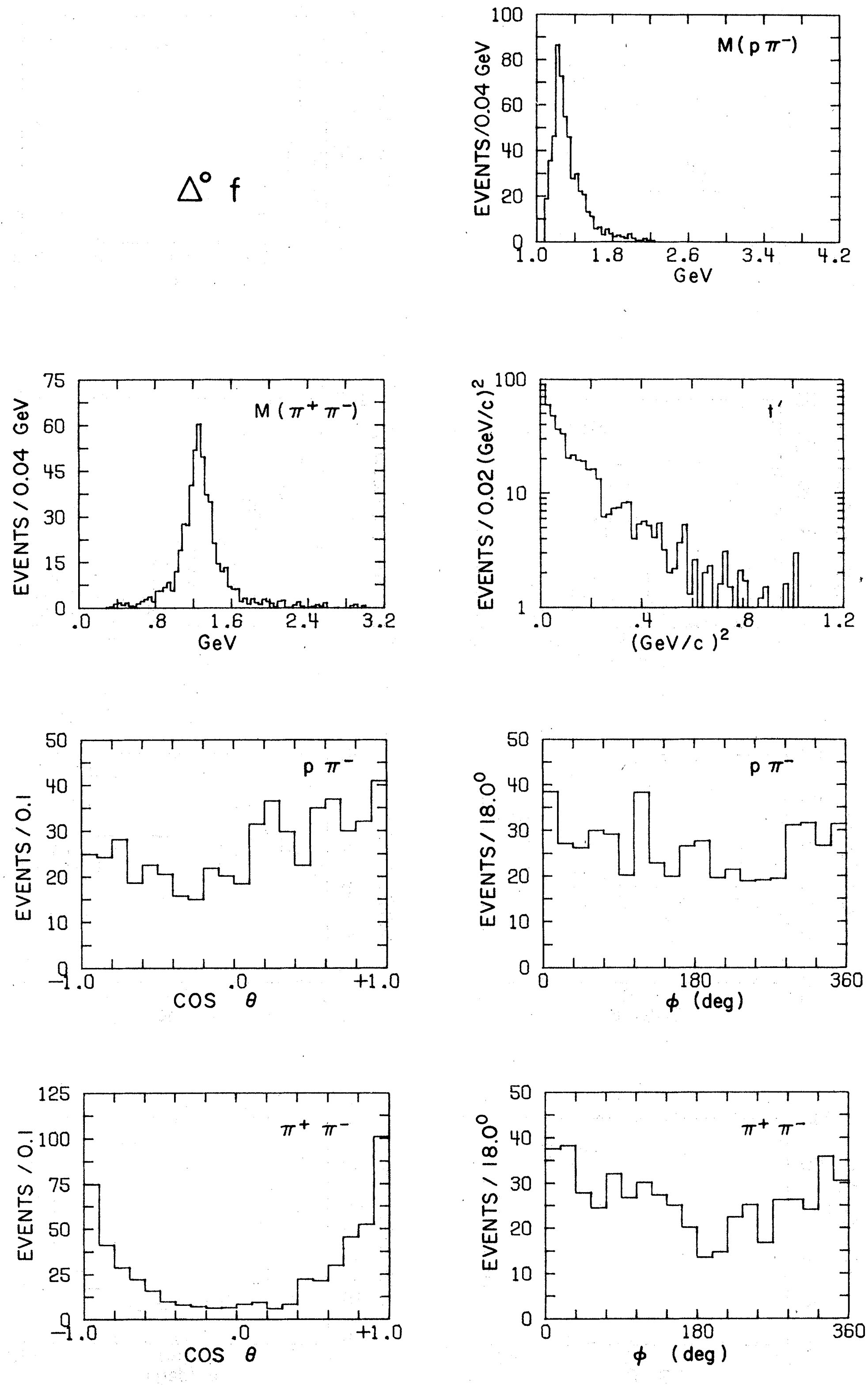

FIG. 9. Effective-mass, momentum-transfer, and decay-angular distributions for the reaction $\pi^- p \rightarrow \Delta^0 f$.

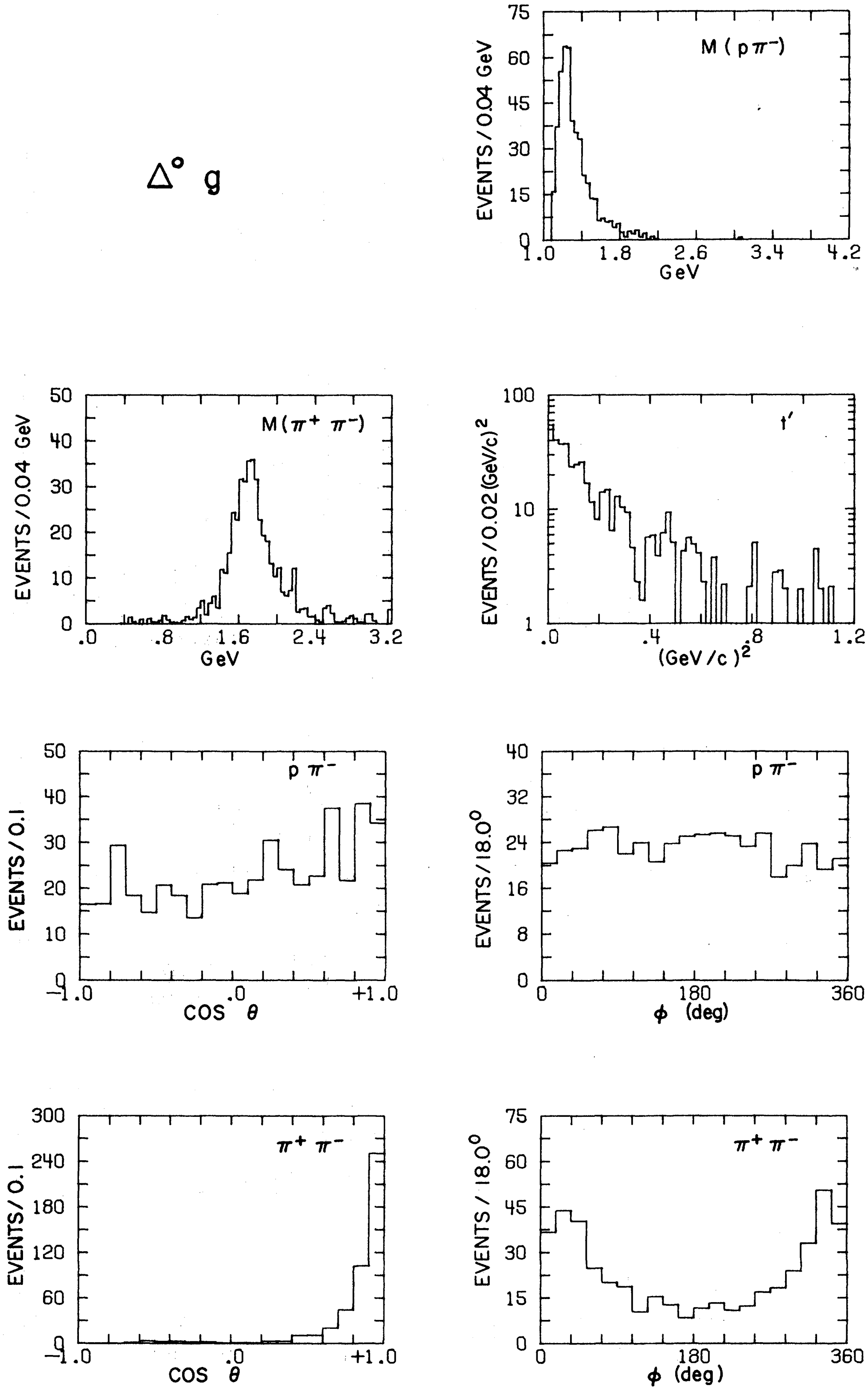

FIG. 10. Effective-mass, momentum-transfer, and decay-angular distributions for the reaction $\pi^- p \to \Delta^0 g$.

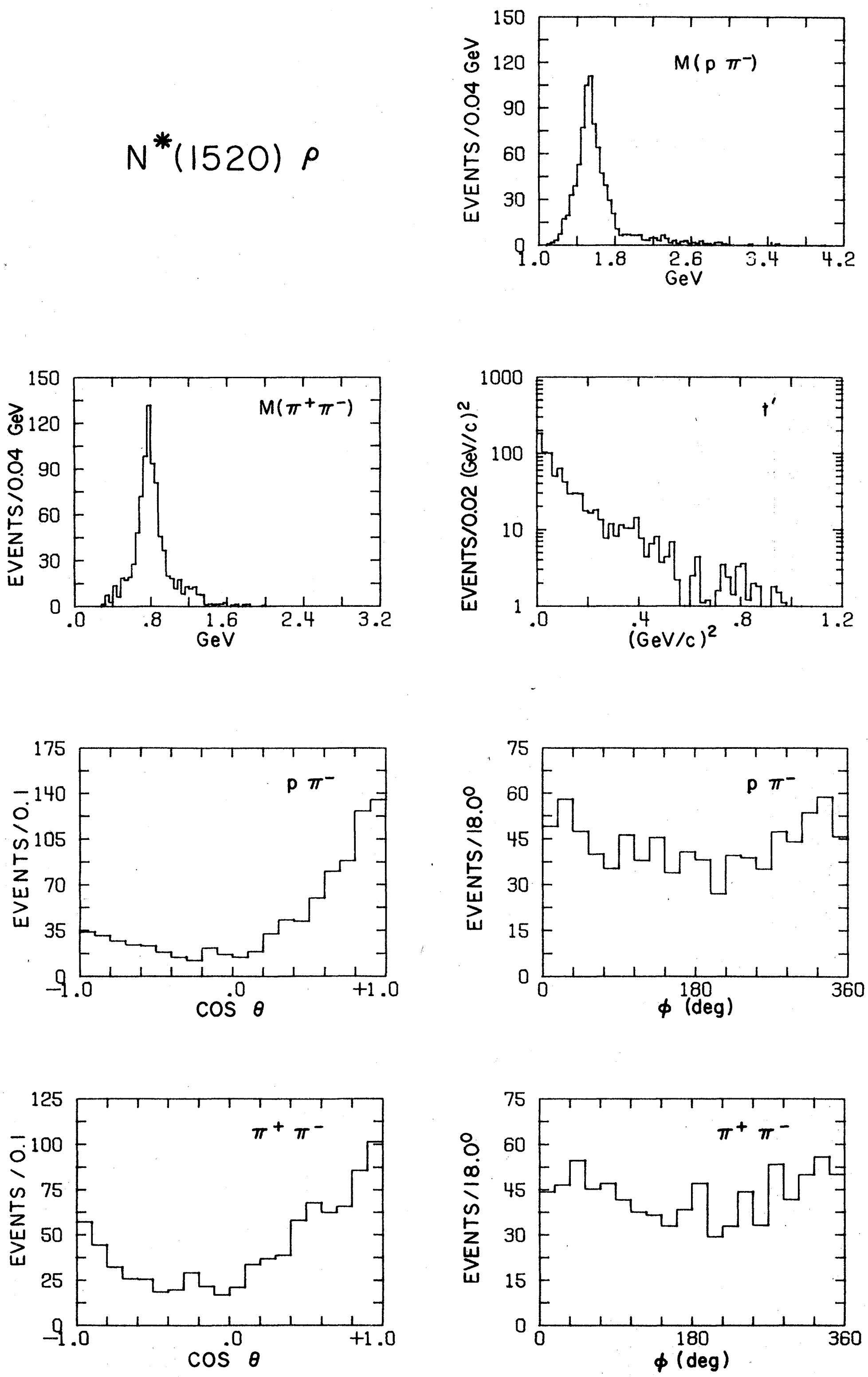

FIG. 11. Effective-mass, momentum-transfer, and decay-angular distributions for the reaction $\pi^- p \rightarrow N^*(1520)\rho^0$.

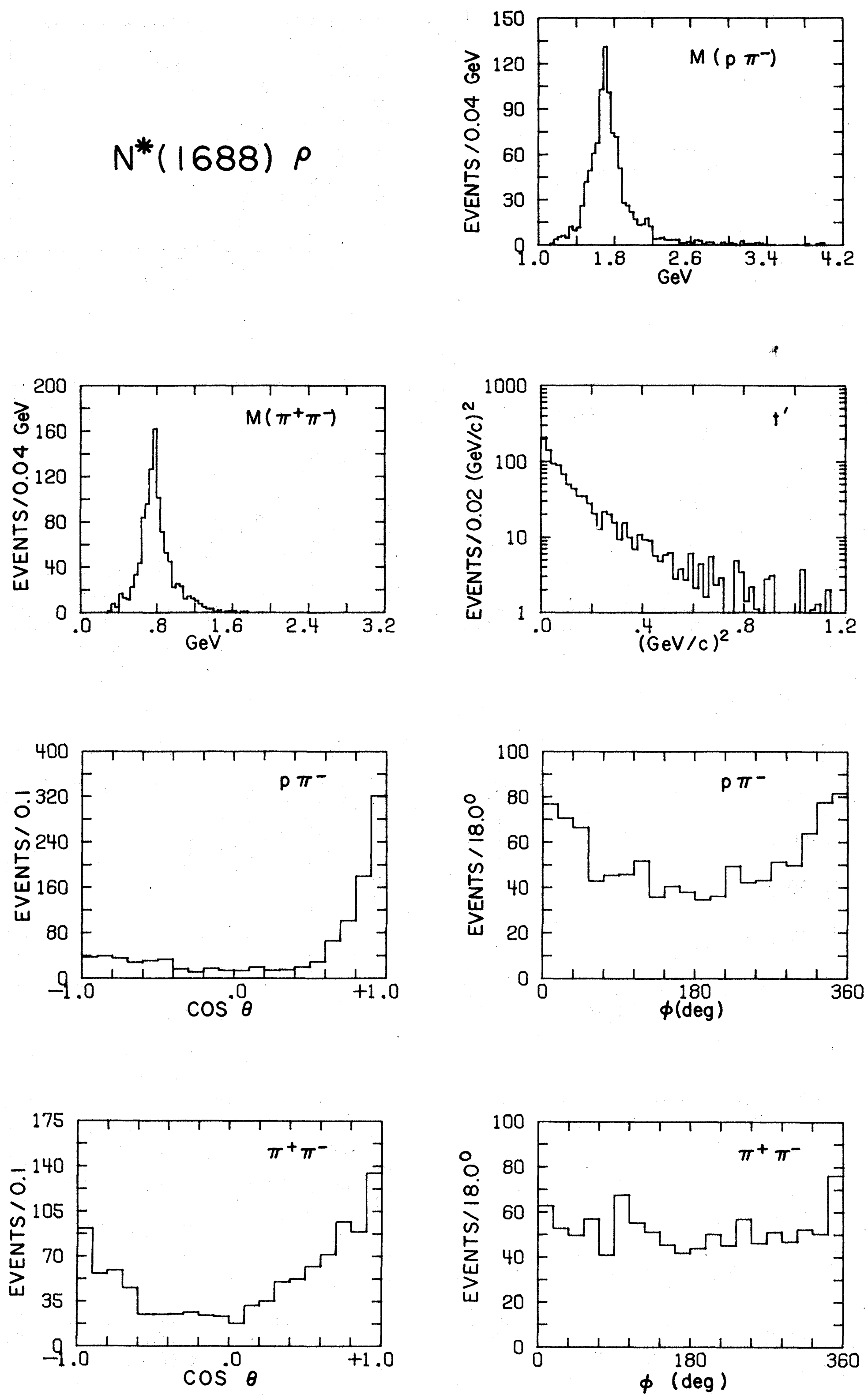

FIG. 12. Effective-mass, momentum-transfer, and decay-angular distributions for the reaction $\pi^- p \to N^*(1688)\rho^0$.

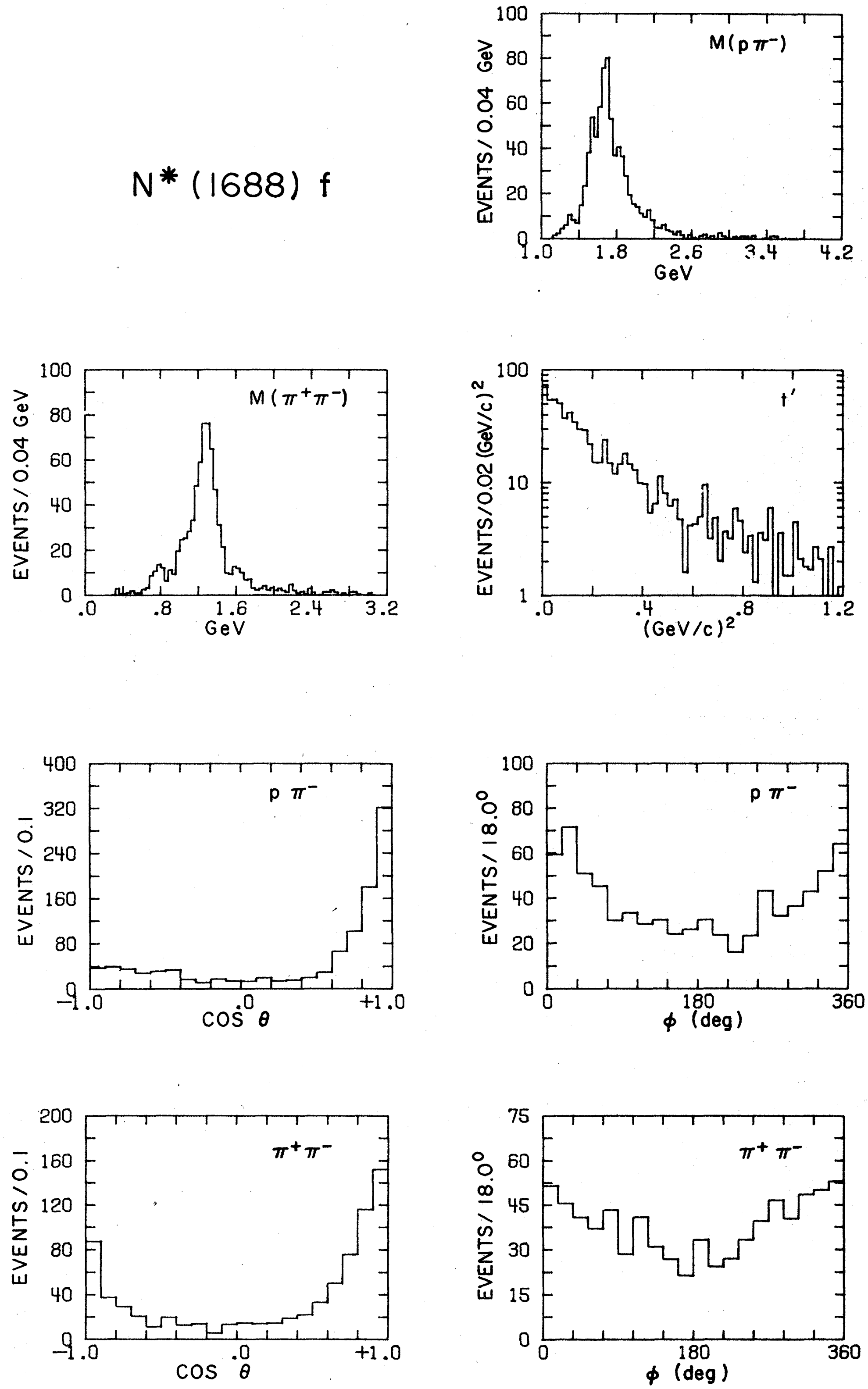

FIG. 13. Effective-mass, momentum-transfer, and decay-angular distributions for the reaction $\pi^- p \rightarrow N^*(1688)f$.

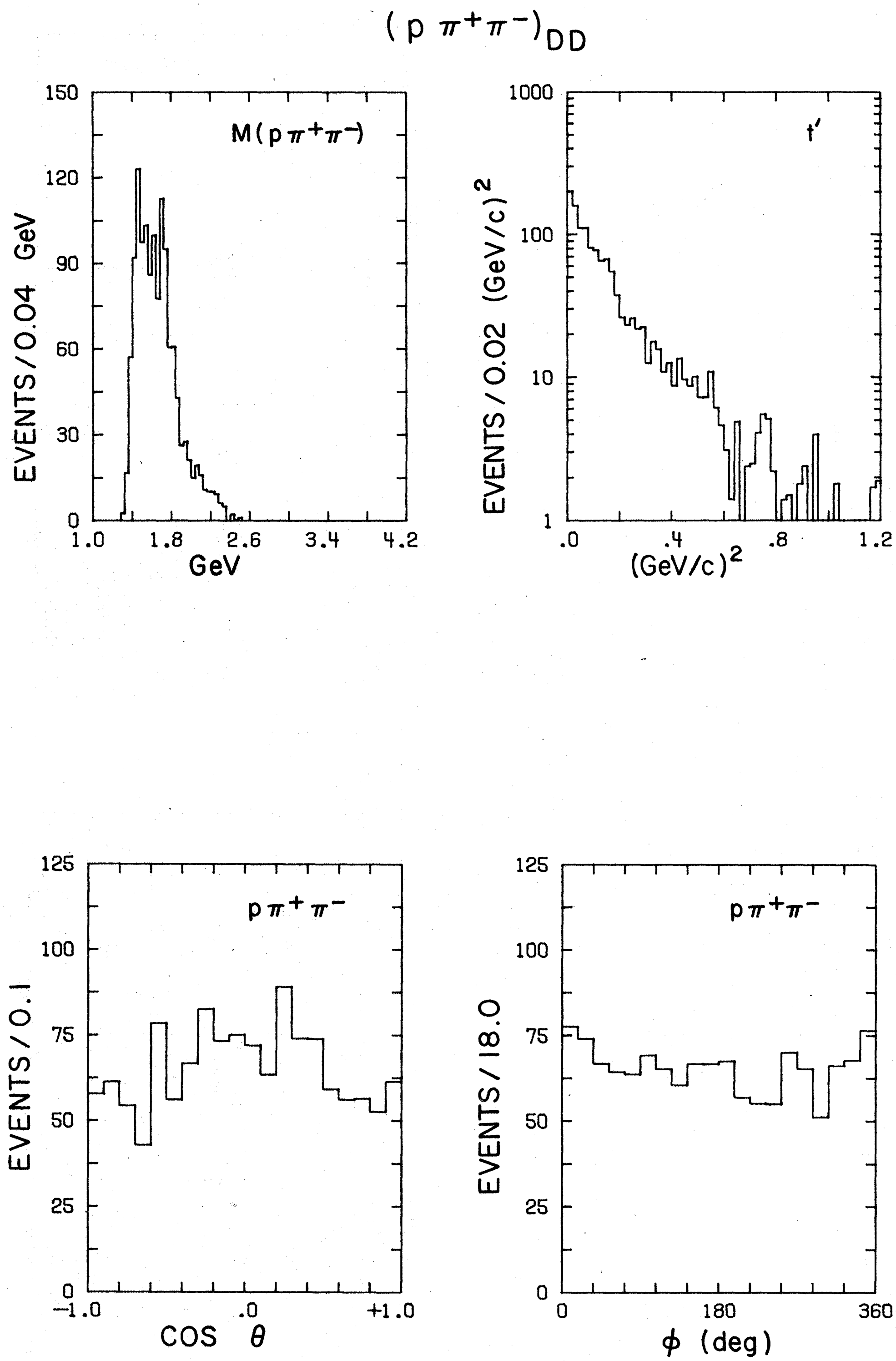

FIG. 14. Effective-mass, momentum-transfer, and decay-angular distributions in the diffractive reaction $\pi^- p \to (p\pi^+\pi^-)_{DD}\pi^-$ for non-Δ^{++} contributions of the $\pi^+ p$.

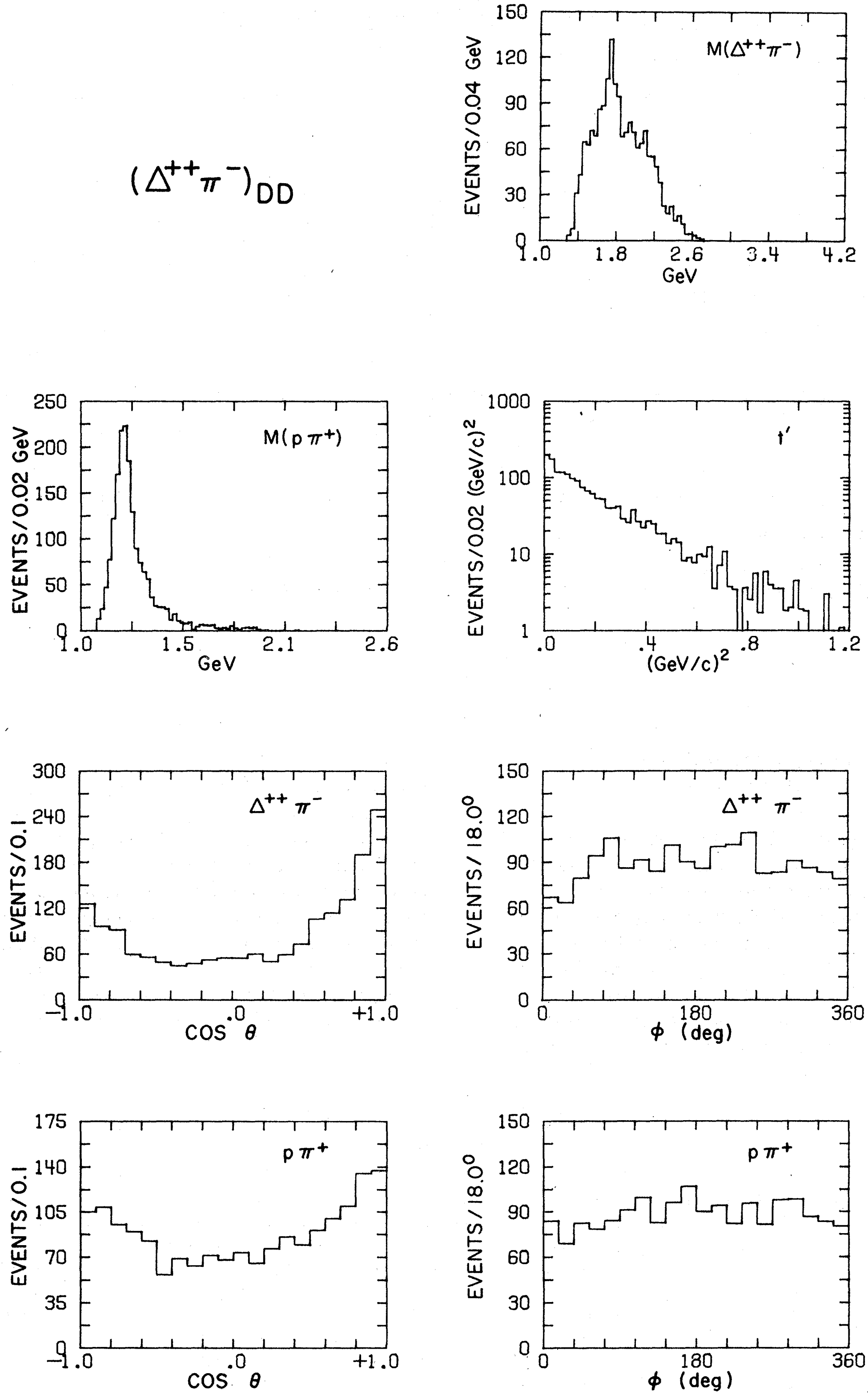

FIG. 15. Effective-mass, momentum-transfer, and decay-angular distributions for the diffractive reaction $\pi^- p \to (\Delta^{++}\pi^-)_{DD}\pi^-$.

TABLE III. Overlap matrix; percentage.

$i \backslash j$	A_1	A_2	A_3	A'	$\Delta^{++}\pi^-\pi^-$	$\Delta^0\pi^+\pi^-$	$\Delta^0\rho^0$	$\Delta^0 f$	$\Delta^0 g$	$N_1\rho^0$ [a]	$N_2\rho^0$ [b]	$N_2 f$	$(P\pi^+\pi^-)_{DD}$	$(\Delta^{++}\pi^-)_{DD}$
A_1		24	3	1	0.5	0.1	1	0.1	0.1	4	7	1	0.1	0.2
A_2	27.0		9	3	1	0.2	2	0.4	0.1	7	10	3	0.1	0.4
A_3	6	15		12	1	1	4	3	0.2	7	11	10	0.3	0.6
A'	2	6	13		8	1	5	3	2	8	8	9	2	4
$\Delta^{++}\pi^-\pi^-$	1	2	2	9		0.4	1	3	4	1	1	4	9	14
$\Delta^0\pi^+\pi^-$	0.5	1	2	3	1		6	9	7	5	3	5	2	2
$\Delta^0\rho^0$	3	6	6	7	1	3		12	3	19	12	6	6	5
$\Delta^0 f$	0.4	1	4	5	4	6	12		13	7	4	13	13	12
$\Delta^0 g$	0.1	0.2	0.3	3	5	4	4	14		1	1	4	24	19
$N_1\rho^0$	8	12	7	7	1	2	12	4	1		28	10	2	3
$N_2\rho^0$	13	16	9	6	1	1	6	2	0.5	23		9	1	3
$N_2 f$	2	5	12	10	4	2	5	9	3	11	13		3	7
$(p\pi^+\pi^-)_{DD}$	0.1	0.1	0.3	1	7	1	3	7	13	2	1	3		37
$(\Delta^{++}\pi^-)_{DD}$	0.3	1	0.4	2	9	1	2	5	8	2	2	4	30	

[a] $N_1 = N^*(1520)$.
[b] $N_2 = N^*(1688)$.

V. COMPARISON WITH OTHER SEPARATION TECHNIQUES

As we mentioned earlier, the reaction $\pi^- p \to \pi^-\pi^-\pi^+ p$ has been studied over a wide range of energies using different methods of investigation. A comparison between different analyses should therefore take into account the special method which has been used to identify and separate contributing channels. In Table V., we present a survey of the most important results obtained in analyzing reaction (1) in the energy range from 8 to 20 GeV/c. Cross sections for strong double resonance channels have similar values regardless of measurement technique whereas less conspicuous reactions require a PPA-type analysis for resolvement; in particular, the A'(2000), which is not readily observed in the raw data, emerges from the PPA technique. Although pion and proton diffractive reactions require a detailed partial-wave analysis for separating interfering states, the general isolation is consistent among techniques when summed over contributing subchannels.

TABLE IV. Slope parameter in $\exp(bt')$ fit for two $|t'|$ intervals, in units of $(\mathrm{GeV}/c)^{-2}$.

Channel	$0<\lvert t'\rvert<0.1\ (\mathrm{GeV}/c)^2$	$0<\lvert t'\rvert<0.4\ (\mathrm{GeV}/c)^2$	Channel	$0<\lvert t'\rvert<0.1\ (\mathrm{GeV}/c)^2$	$0<\lvert t'\rvert<0.4\ (\mathrm{GeV}/c)^2$
A_1	9.6 ± 0.8	11.3 ± 0.2	$\Delta^0 f$	13.2 ± 2.2	7.9 ± 0.5
A_2	4.2 ± 1.2	6.0 ± 0.2	$\Delta^0 g$	8.4 ± 2.6	6.6 ± 0.6
A_3	3.0 ± 1.6	5.9 ± 0.3	$N_1\rho^0$	14.8 ± 1.6	8.8 ± 0.4
A'	6.4 ± 1.7	6.4 ± 0.3	$N_2\rho^0$	14.3 ± 1.5	9.1 ± 0.4
$\Delta^{++}\pi^-\pi^-$	21.1 ± 1.4	13.1 ± 0.4	$N_2 f$	7.1 ± 2.2	5.0 ± 0.4
$\Delta^0\pi^+\pi^-$	6.6 ± 4.5	3.3 ± 0.8	$(p\pi^+\pi^-)_{DD}$	11.0 ± 1.4	8.0 ± 0.3
$\Delta^0\rho^0$	21.3 ± 1.9	12.6 ± 0.5	$(\Delta^{++}\pi^-)_{DD}$	8.1 ± 1.3	5.6 ± 0.3

TABLE V. Reaction cross sections and method of determination. PWA: partial-wave analysis, PPA: prism-plot analysis, ML: maximum likelihood, CA: cluster analysis. Method not indicated implies kinematical selection.

	P(beam) (GeV/c)	σ (μb)	Method	Ref.
A_1	11	83 ± 18		2
	11	118 ± 22	PWA	5
	11.2	216 ± 45	PWA	13
	13	104 ± 22	PWA	5
	13.2	200 ± 17	PPA	this article
	16	294^{+57}_{-34}	ML	7
	16	96 ± 13		2
	16	431	PPA	15
	16	220 ± 18	CA	27
	20	88 ± 16	PWA	5
	20	130 ± 35		2
A_2	8	42 ± 12		2
	11	27 ± 5	PWA	6
	11	78 ± 18		2
	11	51 ± 16		2
	11.2	46 ± 13	PWA	13
	13	35 ± 8	PWA	6
	13	27 ± 5		2
	13.2	124 ± 13	PPA	this article
	16	23 ± 4	PWA	6
	16	158^{+34}_{-23}	ML	7
	16	72 ± 10		2
	16	50	PPA	15
	16	180 ± 60		2
	16	136 ± 23	CA	27
	16.2	46 ± 10		2
	18.5	24 ± 3		6
	20	24 ± 5		6
	20	15 ± 4		2
A_3	11	37 ± 8	PWA	8
	11	64 ± 15		2
	11.2	64 ± 14	PWA	13
	13	50 ± 9	PWA	8
	13.2	71 ± 9	PPA	this article
	16	39 ± 5	PWA	8
	16	113 ± 25	ML	7
	16	80 ± 14	PPA	15
	16	106 ± 16	CA	27
	18.5	32 ± 5	PWA	8
	20	27 ± 4	PWA	8
A'	13.2	64 ± 9	PPA	this article
	16	56	PPA	15
	16	40 ± 8	CA	27
$\Delta^{++}\pi^-\pi^-$	8	320 ± 50		2
	10.25	100 ± 40		2
	11	320 ± 30		2
	13	275 ± 28		2
	13.2	67 ± 9	PPA	this article
	16	44 ± 10	PPA	15
	16	123 ± 22	ML	7
	16	240 ± 50		2
	16	182 ± 12		2
	16	80 ± 19	CA	27

TABLE V. *(Continued).*

	P(beam) (GeV/c)	σ (μb)	Method	Ref.
$\Delta^0\pi^+\pi^-$	11	150 ± 50		2
	13	180 ± 34		2
	13.2	17 ± 5	PPA	this article
	16	45 ± 11	ML	7
	16	50 ± 20		2
	16	0	CA	27
	20	124 ± 21		2
	20	46 ± 6		2
$\Delta^0\rho^0$	8	28 ± 7		2
	11	50 ± 15		2
	13.2	39 ± 7	PPA	this article
	16	30 ± 15		2
	20	4 ± 2		2
	20	30		2
$N_1\rho$	2.7	60		2
	3.7	75 ± 25		2
	13.2	54 ± 8	PPA	this article
	16	48 ± 10	CA	27
Δ^0f	13.2	33 ± 6	PPA	this article
	16	11 ± 4	CA	27
Δ^0g	13.2	29 ± 6	PPA	this article
$N_2\rho^0$	3.7	78 ± 25		2
	13.2	65 ± 9	PPA	this article
	20	9 ± 2		2
N_2f	13.2	47 ± 7	PPA	this article
$(p\pi^+\pi^-)_{DD}$	11.9	80 ± 30		10
	13.2	81 ± 10	PPA	this article
	16	166	PPA	15
$(\Delta^{++}\pi^-)_{DD}$	11.9	220 ± 30		10
	13.2	110 ± 12	PPA	this article
	14.2	226 ± 25		14
	16	147	PPA	15

VI. CONCLUSION

For noninterfering reaction channels occurring in separate regions of phase space, the PPA technique provides an excellent tool for scanning the phase volume and tagging individual events. This procedure resolves the rarer resonant states and provides a reasonably clean data sample for a partial-wave decomposition of the diffractive excitation modes. Some 96% of this four-particle final state was tagged with respect to specific reaction channels. Our conclusion is that the reaction $\pi^-p\rightarrow\pi^-\pi^-\pi^+p$ can be described totally in terms of resonant and diffractive final states.

ACKNOWLEDGMENTS

The authors wish to thank Professor I. A. Pless for a copy of the MIT PPA program and Doctor M. F. Hodus and T. Lainis for useful discussions. We also acknowledge the assistance of Doctors R. S. Dulude and R. J. DeBonte and A. R. Moser in facilitating the use of the PPA at Purdue; we thank A. D. MacKenzie for preparing the figures. This research was supported in part by the U. S. Energy Research and Development Administration.

[1]J. E. Brau, F. T. Dao, M. F. Hodous, I. A. Pless, and R. A. Singer, Phys. Rev. Lett. 27, 1481 (1971); F. T. Dao, M. F. Hodous, I. A. Pless, and R. A. Singer, MIT PEPR Programming note Physics 101, 1971 (unpublished); H. E. Haber and I. A. Pless, MIT PEPR Programming Note Physics 102, 1973 (unpublished).

[2]For results published before 1970, see the compilation by E. Bracci *et al.*, CERN Report No. CERN/HERA 72-1 (unpublished).

[3]T. F. Johnston *et al.*, Nucl. Phys. B24, 253 (1970).

[4]J. Ballam *et al.*, Phys. Rev. D 4, 1946 (1971).

[5]G. Ascoli *et al.*, Phys. Rev. Lett. 26, 929 (1971).

[6]G. Ascoli *et al.*, report submitted to the XVI International Conference on High Energy Physics, Batavia, Illinois, 1972 (unpublished).

[7]R. Honecker *et al.*, Aachen-Berlin-Bonn-CERN-Heidelberg Collaboration, Nucl. Phys. B50, 157 (1972).

[8]G. Ascoli *et al.*, Phys. Rev. D 7, 669 (1973).

[9]Y. M. Antipov *et al.*, CERN-IHEP Boson Spectrometer Group, Nucl. Phys. B63, 141 (1973); B63, 153 (1973).

[10]A. D. Johnson *et al.*, Phys. Rev. D 7, 1314 (1973).

[11]S. Lichtman *et al.*, Nucl. Phys. B81, 31 (1974).

[12]H. H. Bingham *et al.*, Berkley-Fermilab Collaboration, Phys. Lett. 51B, 397 (1974).

[13]G. Thompson *et al.*, Bologna-Florence-Genoa-Milan-Oxford-Pavia Collaboration, Nucl. Phys. B101, 285 (1975).

[14]W. Ochs *et al.*, Nucl. Phys. B102, 405 (1976).

[15]H. Graessler *et al.*, Aachen-Berlin-Bonn-CERN-Cracow-Heidelberg-Warsaw Collaboration, Nucl. Phys. B113, 365 (1976).

[16]L. Van Hove, Phys. Lett. 28B, 429 (1969); Nucl. Phys. B9, 331 (1969); A. Bialas *et al.*, *ibid.* B11, 479 (1969).

[17]G. Berland *et al.*, Nucl. Phys. B75, 93 (1974); B78, 29 (1974); B103, 12 (1976).

[18]B. Haber *et al.*, Phys. Rev. D 10, 1387 (1974); R. A. Singer, MIT PhD. Thesis, 1972 (unpublished).

[19]M. Deutschmann *et al.*, Aachen-Berlin-Bonn-CERN-Cracow-Heidelberg Collaboration, Nucl. Phys. B86, 221 (1975).

[20]M. Deutschmann *et al.*, Aachen-Berlin-Bonn-CERN-Cracow-Heidelberg-Warsaw Collaboration, Nucl. Phys. B99, 397 (1975).

[21]T. Lainis *et al.*, Bull. Am. Phys. Soc. 22, 603 (1977); P. A. Miller *et al.*, *ibid.* 22, 602 (1977).

[22]A. Ferrando *et al.*, Nucl. Phys. B135, 237 (1978).

[23]G. Ascoli *et al.*, Phys. Rev. Lett. 25, 962 (1970).

[24]J. W. Lamsa, C. R. Ezell, J. A. Gaidos, and R. B. Willmann, Nucl. Phys. B41, 388 (1972).

[25]G. Thompson, J. A. Gaidos, R. L. McIlwain, and R. B. Willmann, Phys. Rev. D 9, 560, (1974).

[26]G. Otter *et al.*, Aachen-Berlin-Bonn-CERN-Heidelberg Collaboration, Nucl. Phys. B80, 1 (1974).

[27]R. Honecker *et al.*, Aachen-Berlin-Bonn-CERN-Cracow-Heidelberg-Warsaw Collaboration, Nucl. Phys. B (to be published).